Essential Role of Conserved Arginine 160 in Intramolecular Electron Transfer in Human Sulfite Oxidase†

Changjian Feng,‡ Heather L. Wilson,§ John K. Hurley,|| James T. Hazzard,|| Gordon Tollin,*,|| K. V. Rajagopalan,*,§ and John H. Enemark*,‡

Department of Chemistry and Department of Biochemistry and Molecular Biophysics, University of Arizona, Tucson, Arizona 85721, and Department of Biochemistry, Duke University Medical Center, Durham, North Carolina 27710

Received June 13, 2003; Revised Manuscript Received August 27, 2003

ABSTRACT: Arginine 160 in human sulfite oxidase (SO) is conserved in all SO species sequenced to date. Previous steady-state kinetic studies of the R160Q human SO mutant showed a remarkable decrease in $k_{cat}/K_m^{sulfite}$ of nearly 1000-fold, which suggests that Arg 160 in human SO makes an important contribution to the binding of sulfite near the molybdenum cofactor [Garrett, R. M., Johnson, J. L., Graf, T. N., Feigenbaum, A., Rajagopalan, K. V. (1998) *Proc. Natl. Acad. Sci. U.S.A. 95*, 6394−6398]. In the crystal structure of chicken SO, Arg 138, the equivalent of Arg 160 in human SO, is involved in the formation of a positively charged sulfite binding site [Kisker, C., Schindelin, H., Pacheco, A., Wehbi, W., Garnett, R. M., Rajagopalan, K. V., Enemark, J. H., Rees, D. C. (1997) *Cell 91*, 973−983]. To further assess the role of Arg 160 in human SO, intramolecular electron transfer (IET) rates between the reduced heme [Fe(II)] and oxidized molybdenum [Mo(VI)] centers in the wild type, R160Q, and R160K human SO forms were investigated by laser flash photolysis. In the R160Q mutant, the IET rate constant at pH 6.0 was decreased by nearly 3 orders of magnitude relative to wild type, which indicates that the positive charge of Arg 160 is essential for efficient IET in human SO. Furthermore, the IET rate constant for the R160K mutant is about one-fourth that of the wild type enzyme, which strongly indicates that it is the loss of charge of Arg 160, and not its precise location, that is responsible for the much larger decrease in IET rates in the R160Q mutant. Steady-state kinetic measurements indicate that IET is rate-limiting in the catalytic cycle of the R160Q mutant. Thus, the large decrease in the IET rate constant rationalizes the fatal impact of this mutation in patients with this genetic disorder.

In vertebrates the molybdoenzyme sulfite oxidase (SO, EC1.8.3.1)[1] catalyzes the oxidation of sulfite to sulfate with the concomitant reduction of two equivalents of ferricytochrome *c* (cyt *c*)$_{ox}$ (*1*−*3*), according to the following equation:

$$SO_3^{2-} + H_2O + 2\ (\text{cyt } c)_{ox} \rightleftharpoons SO_4^{2-} + 2\ (\text{cyt } c)_{red} + 2H^+ \quad (1)$$

This is the final step in the oxidative degradation of sulfur-containing amino acids, such as cysteine or methionine, and is physiologically essential. The most extensively studied examples of native SO are from rat, human, and chicken livers, and all three enzymes show a very high degree of sequence similarity (*1*).

Sulfite oxidase deficiency is a devastating genetic disease in humans, with no effective therapies known (*4*). The disorder is characterized by dislocation of ocular lenses, mental retardation, and in severe cases, attenuated growth of the brain (*5*) and early death. These severe neurological symptoms result from either the inability to properly produce the pyranopterindithiolate cofactor, which results in simultaneous deficiencies in all mononuclear Mo enzymes, or from point mutations in the SO protein itself (*2*). The biochemical basis of the pathology of sulfite oxidase deficiency is not yet known. Fatal brain damage may be due to the accumulation of a toxic metabolite (possibly SO_3^{2-}); alternatively, a deficiency in the reaction product (SO_4^{2-}) may disturb normal fetal and neonatal development of the brain (*2*). So far, several point mutations in the structural gene for human SO have been identified in patients with isolated sulfite oxidase deficiency (*6*−*10*). An R160Q mutation at the substrate binding site of human SO, is lethal, and has been identified in several infants worldwide (*6*, *9*, *10*). Previous steady-state kinetic studies of the R160Q human SO mutant showed that both the $K_m^{sulfite}$ and k_{cat} are markedly affected, leading to a decrease in $k_{cat}/K_m^{sulfite}$ of roughly 3 orders of magnitude (*10*). These findings, along with the location of the equivalent

† This work was supported by grants GM 37773 to J.H.E., DK 15057 to G.T. and GM 44283 to K.V.R. from the National Institutes of Health.

* Corresponding authors: John H. Enemark, E-mail: jenemark@u.arizona.edu, phone: 520-626-8065, fax: 520-626-8065; Gordon Tollin, E-mail: gtollin@u.arizona.edu, fax: 520-621-9288; K. V. Rajagopalan, fax: 919-684-8919, E-mail: raj@biochem.duke.edu.

‡ Department of Chemistry, University of Arizona.

§ Department of Biochemistry, Duke University Medical Center.

|| Department of Biochemistry and Molecular Biophysics, University of Arizona.

[1] Abbreviations: CEPT, coupled electron proton transfer; (cyt *c*)$_{ox}$ and (cyt *c*)$_{red}$; ferricytochrome *c* and ferrocytochrome *c*, respectively; dRF and dRFH•: 5-deazariboflavin and 5-deazariboflavin semiquinone, respectively; ET, electron transfer; IET, intramolecular electron transfer; k_{et}, rate constant for intramolecular electron transfer; SO, sulfite oxidase; wt, wild type.

10.1021/bi0350194 CCC: $25.00
Published on Web 10/01/2003

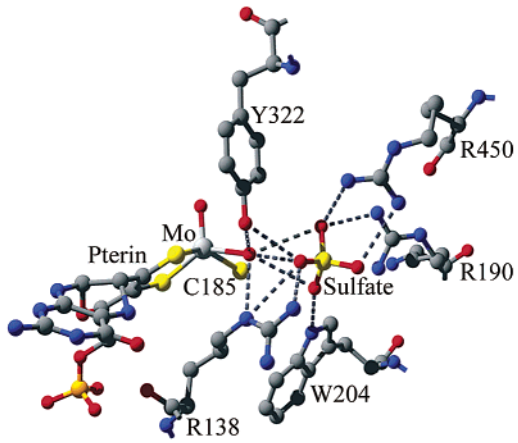

FIGURE 1: The arrangement of amino acids and ligands near the Mo center of chicken SO. For coordinated C185, only the sulfur atom is shown for clarity. Dotted lines indicate selected hydrogen bonds. Arg 138 in chicken SO is the equivalent of Arg 160 in human SO. Coordinates for this figure are from the Brookhaven Protein Data Bank (PDB entry: 1SOX). Figure 1 was generated with Swiss-PdbViewer 3.7 (http://www.expasy.org/spdbv/) and rendered with POVRAY 3.5 (http://www.povray.org).

Arg 138 group at the active site of chicken SO (*11*), strongly suggest that this residue makes an important contribution to the juxtaposition of sulfite to the Mo center of the enzyme.

The X-ray crystal structure of chicken liver SO has recently been reported (*11*). The α_2 dimeric protein consists of an N-terminal b_5-type cytochrome domain and two larger domains that constitute the central molybdenum binding and the C-terminal dimerization domains. The molybdenum center is coordinated by five ligands with approximate square pyramidal coordination geometry. The terminal oxo group occupies the axial position of the pyramid, and the equatorial positions are occupied by three sulfur atoms and one water/hydroxo ligand (Figure 1). As expected for binding an anionic substrate, the sulfite-binding pocket is highly positively charged and consists of three arginines (Arg 138, Arg 190, and Arg 450), Trp 204, and Tyr 322. Arg 138 also forms a hydrogen bond to the equatorial water/hydroxo group (Figure 1). This arginine residue is conserved in all SO from animals (*12*), plants (*13*), bacteria (*14*), and the assimilatory nitrate reductase from eukaryotes (*15*).

In the generally accepted catalytic cycle for SO in vertebrates (Figure 2) (*16*, *17*), the Mo(VI) center of the fully oxidized SO reacts with sulfite to produce sulfate. The two-electron reduced SO, which is in the Mo(IV)/Fe(III) state, undergoes intramolecular electron transfer (IET) to generate the Mo(V)/Fe(II) state that can be detected by electron paramagnetic resonance (EPR) spectroscopy (*18*−*21*). One-electron transfer to exogenous (cyt *c*)$_{ox}$, leaving the enzyme in the one-electron reduced state Mo(V)/Fe(III), accomplishes reoxidation of the Fe(II) center. A second Mo → Fe IET step (giving Mo(VI)/Fe(II)), followed by reduction of a second equivalent of (cyt *c*)$_{ox}$, regenerates the enzyme to the fully oxidized resting state Mo(VI)/Fe(III).

As a two-domain multiredox-center enzyme, IET between the Mo and Fe centers of SO is fundamental to the function of the enzyme. We have previously shown that exogenous flavin radicals generated in situ with a laser pulse will rapidly reduce the heme center of SO by one electron (see the dotted

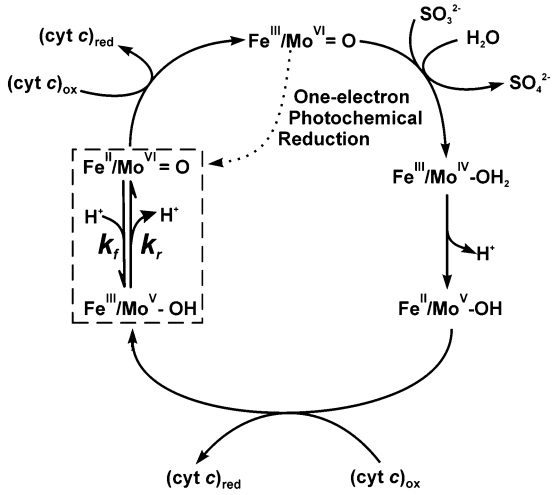

FIGURE 2: Postulated oxidation state changes occurring at the Mo and Fe centers of SO in vertebrates during the catalytic oxidation of sulfite and the concomitant reduction of (cyt *c*)$_{ox}$. Only the equatorial oxygen atom among the ligands of Mo is shown for clarity. The one-electron reduction indicated by a dotted arrow connecting $Mo^{VI}Fe^{III}$ and $Mo^{VI}Fe^{II}$ can be initiated with a laser pulse in a solution containing dRF and the sacrificial electron donor semicarbazide. The IET step between $Mo^{VI}Fe^{II}$ and $Mo^{V}Fe^{III}$, which is of particular interest in this study, is highlighted in the dashed box. The ensuing equilibrium can thus be observed without creating the intermediate species in the cycle. The rate constants k_f and k_r are defined in the text.

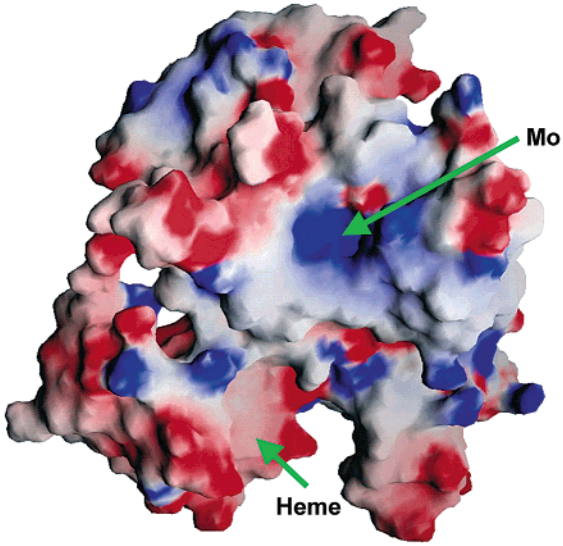

FIGURE 3: Electrostatic surface potentials of chicken SO. Positive potential is shown in blue, and negative potential is shown in red. Electrically neutral surfaces are white. The view is centered on the entrance of the strongly positive charged funnel. Coordinates for this figure are from the Brookhaven Protein Data Bank (PDB entry: 1SOX). Potentials were calculated as described in the text.

arrow in Figure 2), and have used this powerful technique to investigate IET between the Mo and Fe centers in chicken SO as a function of pH and anion concentration (*22*−*24*), and solution viscosity (*25*). Note that this process corresponds to the second physiologically essential IET step mentioned above.

Upon the basis of the crystal structure of chicken SO (*11*), the calculated electrostatic surface potential of chicken SO reveals a highly positively charged funnel that leads from the protein surface to the Mo center (blue region in Figure 3), and Arg 138 is at the entrance of this funnel. Surrounding

this positively charged funnel is an electrically neutral environment (white region in Figure 3), and lying more peripherally is a ring of negatively charged residues (red region in Figure 3). The net effect of this distribution of charged amino acid side chains is to create an "electrostatic bulls-eye", which in both a repulsive (negative − negative) and an attractive (plus − minus) manner, could act to guide the small anionic substrate and the negatively charged exposed heme edge region precisely to the Mo active site. The combination of the IET kinetic information (*22*, *25*) and the surface potential calculation suggests that electrostatic interactions may play a major role in creating "productive" conformations that facilitate rapid IET between the two metal centers (*25*, *26*). There are numerous biological electron transfer (ET) systems whose function depends on the recognition, optimal orientation, and proper interaction between proteins that shuttle electrons (*27*, *28*). Electrostatic interactions between amino acid side chains on protein surfaces play important roles in molecular recognition, making it an active determinant of ET kinetics in redox proteins, and the effect of such interactions on protein ET has produced much interest recently (*28*−*34*).

Human (*35*−*37*) and rat (*38*) SO have been successfully cloned and expressed in highly active forms in *Escherichia coli*. Expression of these proteins makes possible the use of site-directed mutagenesis to incisively probe the roles of specific residues in the function of SO. Recent detailed studies on IET in the Y343F human SO mutant have provided direct evidence of the vital role of Tyr 343 in an efficient coupled electron proton transfer (CEPT) process (*39*). For human SO, the combination of unique rapid kinetic methods such as flash photolysis with site-directed mutagenesis can critically evaluate the involvement of specific amino acid residues in pathological human SO deficiencies. To better understand why the R160Q mutation may be fatal to young children, we have explored the role of the conserved Arg 160 in human SO (the equivalent of Arg 138 in chicken SO) in IET by comparative flash photolysis studies of the wild type (wt), R160Q, and R160K human SO forms.

EXPERIMENTAL PROCEDURES

Site-Directed Mutagenesis. The R160Q and R160K mutations were introduced into pRG118 as previously described (*10*). The DNA fragments containing the coding sequences were then ligated into the p*Trc*99A expression vector (Amersham). Mutations were verified by sequence analysis performed at the Duke University DNA Analysis facility.

Expression and Purification of Wild Type, R160Q, and R160K Human SO. All human SO proteins were expressed in the TP1000 strain and purified as previously described (*35*, *39*). Fractions exhibiting a A_{414}/A_{280} ratio of 0.96 or greater were then pooled and used in the experiments described in this study. The molybdenum content of purified SO proteins was determined using a Perkin-Elmer Zeeman/3030 atomic absorption spectrometer as previously described (*36*), indicating a Mo/heme ratio of 0.85.

Laser Flash Photolysis Studies. Laser flash photolysis experiments were performed anaerobically on 0.50 mL solutions containing 5-deazariboflavin (dRF) and 0.5 mM freshly prepared semicarbazide as the sacrificial reductant. The laser apparatus and associated visible absorbance detection system have been extensively described (*40*), as has the basic photochemical process by which 5-deazariboflavin semiquinone (dRFH$^{\bullet}$) is generated by reaction between triplet state dRF and the sacrificial reductant and used to reduce redox-active proteins (*41*). Briefly, a N_2 laser (Photochemical Research Associates (PRA), London, Ontario, Canada) was used to pump a dye laser (BBQ 2A368 dye, 396 nm wavelength maximum; PRA), which was focused onto the sample cell. Samples were deaerated by bubbling with H_2O-saturated O_2-free argon for 2 h, prior to addition of microliter volumes of concentrated protein. Where necessary, argon was purged over the surface of the added protein to remove traces of O_2. Experiments were performed at room temperature. Further details concerning the photochemical process, which are of particular relevance to the SO system, are presented below. Generally, data from 6−12 laser flashes were averaged. Transient absorbance changes at 555 nm were analyzed using the computer fitting procedure SIFIT, obtained from OLIS Inc. (Jefferson, GA).

Steady-State Kinetic Studies. Steady-state enzyme kinetic studies were performed aerobically in a Varian Cary-300 spectrophotometer. Initial velocities were determined by following the reduction of a freshly prepared oxidized cytochrome *c* (type VI, Sigma-Aldrich Co.) solution at 550 nm, using an extinction coefficient change of 19 630 M^{-1} cm^{-1} (*42*). The steady-state kinetic study was conducted using a saturating concentration of cytochrome *c* (15 μM) and varying the concentration of sodium sulfite. The buffers used were 100 mM Bis-Tris (pH 6.0), and Bis-Tris propane (pH 7.4), adjusted to the appropriate pH with acetic acid to minimize the possibility of anion inhibition (*43*).

Electrostatic Potential Surface Map. Structures of the chicken SO mutant R138Q and R138K were made by replacement of Arg 138 in the Protein Data Bank file using the software package INSIGHT II (Molecular Simulations, Inc., San Diego, California). Electrostatic potentials for all structures were calculated using DELPHI (Molecular Simulations, Inc.), with an ionic strength of 0.146 M. Mapping of the electrostatic potential onto the molecular surface of the protein was performed using GRASP (*44*), with a potential range of −10 to +10 *kT*.

RESULTS

Photochemical Reduction of Human SO by Deazariboflavin Semiquinone. The photochemical reduction of the Fe(III) heme moiety of human SO was monitored by laser flash photolysis-induced transient absorbance changes. The flash-induced difference spectra of R160Q and R160K human mutants show similar peaks and isosbestic points (data not shown) to those obtained with the wild type human SO (*39*) and native chicken SO (*23*). These spectra confirm that the transient absorbance changes observed at 555 nm are directly related to reduction and reoxidation of the *b*-type heme prosthetic group.

Figure 4 shows a typical transient kinetic trace obtained at 555 nm upon laser flash photoexcitation of a solution containing oxidized R160K human SO, dRF, and semicarbazide. The kinetic behavior can be fully described in terms of the set of reactions shown in eqs 2−5 below. The laser pulse excites 5-deazariboflavin (dRF) to the triplet state (eq

2), which abstracts a hydrogen atom from semicarbazide (AH_2) to form the highly reducing dRF semiquinone radical (dRFH$^\bullet$) (eq 3). The initial positive deflection of absorbance from zero in Figure 4 is due to net reduction of the Fe(III) center to the Fe(II) form (eq 4), which has an absorbance maximum at 555 nm. The slow decrease in absorbance that follows the initial rapid increase is due to the net IET from Fe(II) to Mo(VI), i.e., the heme reoxidation phase, which establishes an equilibrium between the Mo(VI)/Fe(II) and Mo(V)/Fe(III) forms of SO (eq 5). The kinetics of this latter process are independent of the concentration of human SO, indicating that it is due to a intramolecular process, which is the reaction that is of particular interest to us in this study. It is important to note that the IET rates of R160Q and R160K mutants are also independent of protein concentration, consistent with their intramolecular nature.

$$\mathrm{dRF} \xrightarrow{h\nu} {}^1\mathrm{dRF} \rightarrow {}^3\mathrm{dRF} \quad (2)$$

$${}^3\mathrm{dRF} + \mathrm{AH_2} \rightarrow \mathrm{dRFH}^\bullet + \mathrm{AH}^\bullet \quad (3)$$

$$\mathrm{dRFH}^\bullet + \mathrm{Mo(VI)/Fe(III)} \rightarrow \mathrm{dRF} + \mathrm{Mo(VI)/Fe(II)} \quad (4)$$

$$\mathrm{Mo(VI)/Fe(II)} \underset{k_r}{\overset{k_f}{\rightleftharpoons}} \mathrm{Mo(V)/Fe(III)} \quad (5)$$

For the case shown in Figure 4, in which the flash-induced reduction of SO occurs much faster than subsequent IET, values for the overall IET rate constant k_{et} ($= k_f + k_r$) and parameters *a* and *b* can be obtained by fitting the heme reoxidation phase with the exponential function given in eq 6 (the meanings of the parameters *a* and *b* are shown in Figure 4).

$$A_{555} = a + b \exp(-k_{et}\, t) \quad (6)$$

On the basis of eq 5, the parameters *a* and *b* in eq 6 have the meanings given in eqs 7 and 8 (where A_0 is simply the absorbance extrapolated to $t = 0$, assuming that the photochemically induced reduction of SO is instantaneous).

$$a = \mathrm{A_0}\frac{\mathrm{k_r}}{\mathrm{k_{et}}} = \mathrm{A_0}\frac{\mathrm{k_r}}{\mathrm{k_f} + \mathrm{k_r}} \quad (7)$$

$$b = \mathrm{A_0}\frac{k_f}{\mathrm{k_{et}}} = \mathrm{A_0}\frac{k_f}{k_f + k_r} \quad (8)$$

$$K_{eq} = \frac{k_f}{k_r} = \frac{b}{a} \quad (9)$$

Thus, the individual IET rate constants k_f and k_r can be calculated from k_{et} and K_{eq} ($= b/a$, eq 9). The IET rate constants and K_{eq} values for the wild type and R160Q (Figure 5), and R160K human SO under the same conditions are shown in Table 1. Note the remarkable difference in the time scale of the kinetic traces for the wild type and R160Q human SO (Figure 5).

The Dependence of IET Rates on pH. Figure 6 shows the dependence of the k_f and k_r magnitudes of the R160K human SO on [OH^-] between pH 7.0 and 7.9, in solutions containing

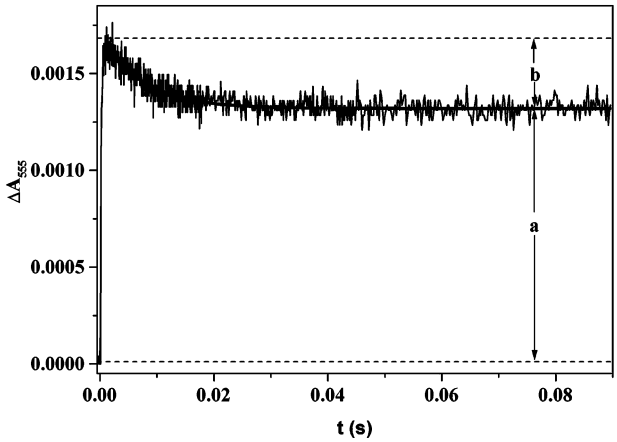

FIGURE 4: Transient kinetic trace obtained at 555 nm upon photoexcitation of a solution containing 10 μM R160K human SO, $\sim$ 90 μM dRF, 6 mM HCl, and 0.5 mM semicarbazide hydrochloride in Tris buffer (pH 7.0). The Tris base concentration was chosen so as to achieve the appropriate pH while keeping [Cl^-] at $\sim$ 6.5 mM. The solid line indicates a single-exponential fit to the IET phase. $K_{eq} = b/a$.

Table 1: Flash Photolysis Kinetic Parameters for the Wild Type (wt), R160Q, and R160K Human SO at pH 6.0[a]

	k_{et} (s^{-1})	K_{eq}
wild type	411 ± 15	0.36 ± 0.02
R160Q	0.64 ± 0.10	0.21 ± 0.05
ratio (wt/R160Q)	642	1.7
R160K	96 ± 8	0.36 ± 0.03
ratio (wt/R160K)	4	1

[a] Solutions contained 0.5 mM semicarbazide hydrochloride, 20 mM Bis-Tris. pH was adjusted to 6.0 with HAc.

low anion concentrations ([Cl^-] $\sim$ 6.5 mM). Note that k_f for the mutant decreases slightly with increasing [OH^-], but k_r is essentially unchanged. Figure 7 shows the effects of pH on K_{eq} for IET in the wild type and R160K human SO. Note the decrease in the K_{eq} values for the R160K mutant compared to the wild type enzyme. Due to the small amplitude of the signal decay due to IET (see Figure 5A), experiments on R160Q could not be conducted over this pH range.

DISCUSSION

IET Rates of the Wild Type, R160Q, and R160K Human SO. As noted above, we attempted to observe IET in the R160Q mutant in the same pH range (approximately 7−8) as for the wild type enzyme. However, no decay after heme reduction due to IET was observed at 555 nm. For this mutant, the Fe^{II} reoxidation phase only began to be detectable at pH 6.0. We presume this is due to an unfavorable equilibrium above this pH. By means of activity measurements, however, it was observed that the R160Q mutant still remains functional at pH 6.0 ($k_{cat} = 0.33\ s^{-1}$). In addition, the magnitudes of the signal change at 555 nm in flash photolysis experiments at this pH were comparable to those observed with the wild type protein at pH 7.4.

At pH 6.0, the k_{et} value of R160Q is only 0.64 s^{-1} (compared to 411 s^{-1} for the wild type under the same conditions, Table 1), which strongly suggests that the positive charge of Arg 160 is critical for rapid IET in human SO. It

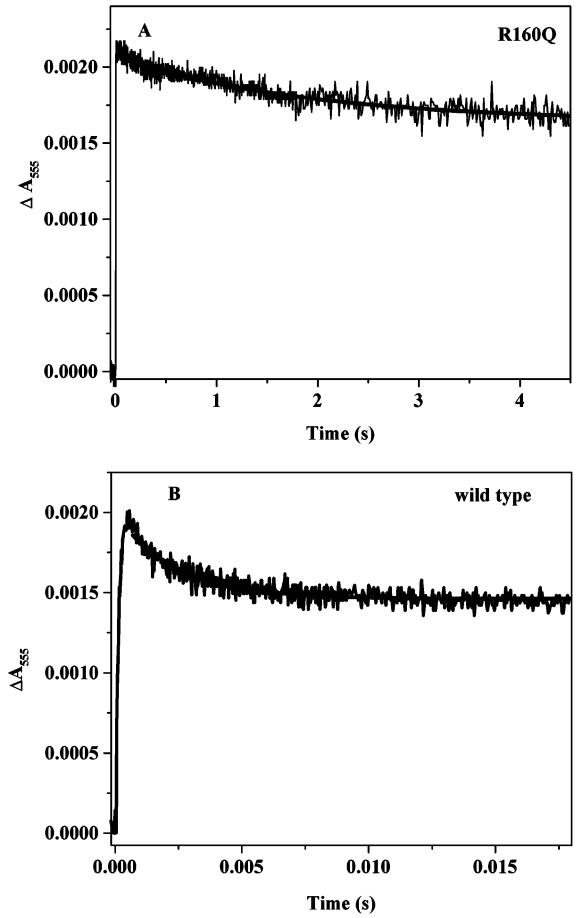

FIGURE 5: Transient kinetic trace obtained at 555 nm upon photoexcitation of a solution containing (A) 11 μM R160Q, or (B) 9 μM wild type human SO, and ~90 μM dRF, and 0.5 mM semicarbazide in 20 mM Bis-Tris. pH was adjusted to 6.0 with HAc. The solid line indicates a single-exponential fit to the IET phase.

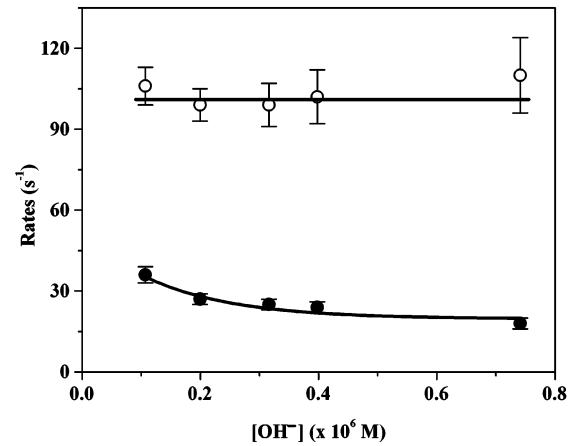

FIGURE 6: Dependence of the rate constants k_f (solid symbols) and k_r (open symbols) of the R160K mutant on hydroxide ion concentration. Solutions contained 0.5 mM semicarbazide hydrochloride, 6 mM HCl. For all experiments, the Tris base concentration was chosen so as to achieve the appropriate pH while keeping [Cl^-] at ~6.5 mM.

is noteworthy that a similar magnitude of ET rate constant decrease due to surface charge mutation has been observed in the reaction between ferredoxin and ferredoxin:$NADP^+$ reductase (*45*). For the R160Q mutant, K_{eq} decreases from 0.36 in the wild type enzyme to 0.21 (Table 1). However,

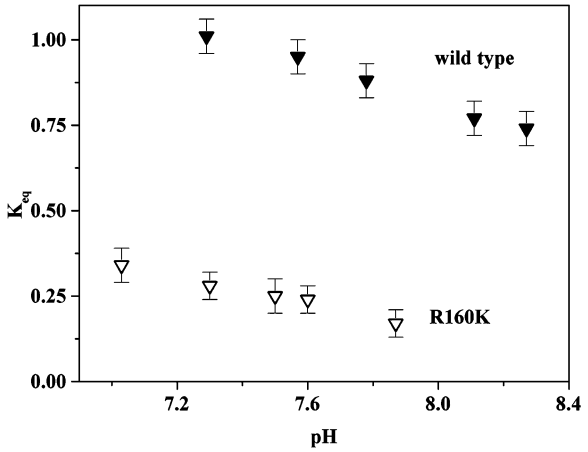

FIGURE 7: Effects of pH on K_{eq} for IET in the wild type (solid symbols) and R160K (open symbols) human SO. The conditions for flash photolysis experiments are the same as shown in the caption of Figure 6.

such a small shift in K_{eq} (i.e., a thermodynamic factor) cannot account for such a large change in the IET rate constant (nearly 3 orders of magnitude). Furthermore, the k_{et} value of the R160K mutant only decreases about 4-fold, being intermediate in value between those of the wild type and the R160Q mutant (Table 1).

Figure 8B,E show that the replacement of Arg 138 by Gln in chicken SO induces a relatively large electrically neutral region close to the Mo center. In contrast, the R138K mutation in chicken SO does not produce a significant change in surface potential character (Figure 8C,F) compared with the wild type (Figure 8A,D), as expected. These data strongly indicate that it is the loss of charge of Arg 160 itself, and not its precise location, that is responsible for the remarkable decrease in the IET rate of the R160Q mutant. In other words, electrostatic interactions involving this residue, play a key role in IET in SO. It is reasonable to surmise that the presence of a positive charge at Arg 160 of human SO may allow the most optimal orientations for IET between the heme and Mo domains (i.e., a kinetic rather than a thermodynamic effect).

At pH 6.0, the k_{cat} value of R160Q is 0.33 s^{-1}, comparable to its k_{et} value (0.64 s^{-1}), suggesting that in this mutant IET may become the rate-limiting step during catalytic turnover. This may seriously retard efficient turnover of toxic sulfite to sulfate, thus helping to rationalize the fatal effect of this mutation. In contrast, in the R160K mutant, at pH 7.4, the values of k_{cat} and k_{et} are 1.4 s^{-1} and 123 s^{-1}, respectively, and at pH 6.0, these values are 0.2 s^{-1} and 96 s^{-1}, respectively, indicating that the IET step in this mutant is not rate-limiting during catalysis, similar to the situation in native chicken SO (*43*) and wild type human SO (*39*). In the Y343F human SO mutant, the IET rate is also much faster than its turnover number (*39*), again suggesting that the IET step is not rate-limiting.

The pH Dependence of IET Rates in the R160K Mutant. The large decrease in K_{eq} for the R160K mutant (Figure 7) indicates that this mutation disfavors the forward IET process (eq 5), which might be due to the weakening of hydrogen-bonding between the equatorial Mo^V-OH group and the nitrogen atom of Arg 160 because of the

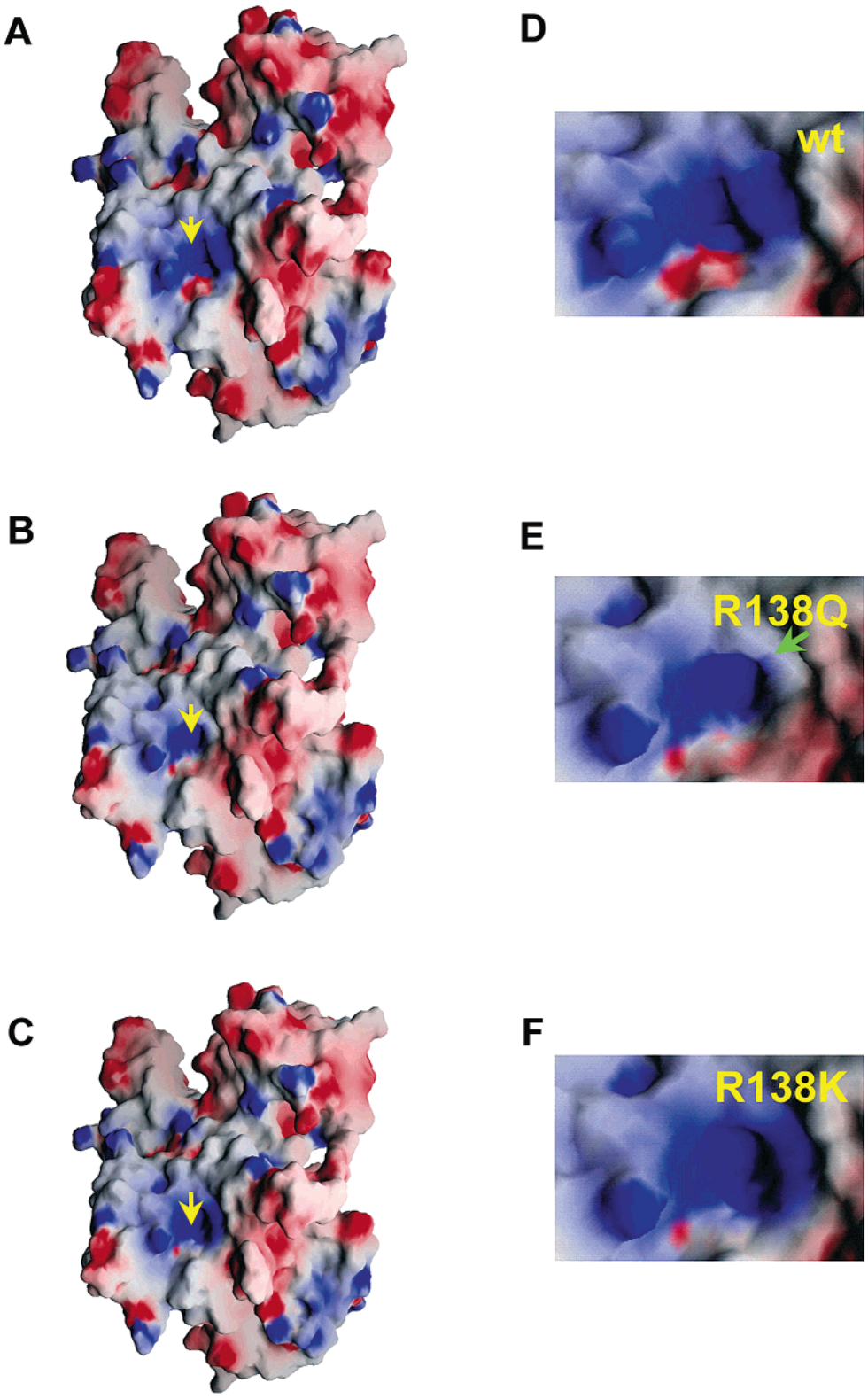

FIGURE 8: (A−C) Electrostatic surface potentials of (A) wild type (wt), (B) R138Q, and (C) R138K chicken SO. Positive potential is shown in blue, and negative potential is shown in red. The view is centered on the entrance of the strongly positive charged funnel, with the position of the Mo center marked by the yellow arrow. (D−F) Closer view of positively charged spot in the Mo active site of (D) wt, (E) R138Q, and (F) R138K. The region of significant changes of charge in R138Q mutant is marked by the green arrow. Coordinates for this figure are from the Brookhaven Protein Data Bank (PDB entry: 1SOX). Potentials were calculated as described in the text.

increase in distance between these moieties (Figure 1). Hydrogen bonding to $Mo^{V}-OH$ can stabilize the +5 oxidation state, thereby making the reduction of Mo^{VI} to Mo^{V} more favorable.

For the R160K mutant, at low anion concentrations, k_f decreases with increasing $[OH^-]$, while k_r is effectively unchanged (Figure 6), which is quite different from the wild type and also from Y343F human SO (*39*). These data can

Scheme 1: Proposed CEPT Mechanism for IET in SO[a]

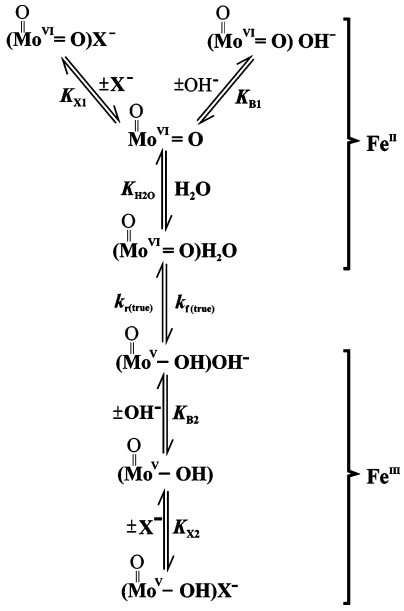

[a] Adapted from ref *22*.

be explained by the previously proposed CEPT mechanism (Scheme 1) (*22*, *39*). Thus, Scheme 1 can be algebraically described by eqs 10 and 11 as follows:

$$k_{\mathrm{f\ app}} = \frac{c}{d + [\mathrm{OH^-}]} \tag{10}$$

where

$$c = \frac{k_{\mathrm{f(true)}} K_{\mathrm{B1}}}{K_{\mathrm{H_2O}}}$$

$$d = K_{\mathrm{B1}}\left(1 + \frac{1}{K_{\mathrm{H_2O}}} + \frac{[\mathrm{X^-}]}{K_{\mathrm{X1}}}\right)$$

$$k_{\mathrm{r\ app}} = \frac{k_{\mathrm{r(true)}}[\mathrm{OH^-}]}{e + [\mathrm{OH^-}]} \tag{11}$$

where

$$e = K_{\mathrm{B2}}\left(1 + \frac{[\mathrm{X^-}]}{K_{\mathrm{X2}}}\right)$$

For R160K, since the parameters d and e are proportional to the dissociation constants K_{B1} and K_{B2} (see Scheme 1 for definitions of K_{B1} and K_{B2}), respectively, it is possible that at sufficiently low values for these two constants, the apparent k_f could decrease with increasing [OH$^-$] (when d is comparable to [OH$^-$]), whereas the apparent k_r could be independent of [OH$^-$] (when $e \ll$ [OH$^-$]), over the entire pH range investigated, as is observed in Figure 6.

In conclusion, this study has provided *direct* experimental evidence for the essential role of a conserved active site arginine (Arg 160 in human SO) in the physiologically critical IET process in SO. In addition, the results provide an experimental rationale for the fatal impact of the R160Q mutant in human disease. A mutation at another positively charged residue near the Mo center in human SO (R211Q) has recently been identified in a patient (*6*). Thus, further flash photolysis studies on this as well as other mutants of cationic residues near the Mo center should provide additional insights into the role of surface charge in IET in SO.

REFERENCES

1. Kisker, C. (2001) in *Handbook of Metalloproteins* (Messerschmidt, A., Huber, R., Poulos, T., and Wieghardt, K., Eds.) Vol. 2, pp 1121−1135, John Wiley & Sons, Ltd., New York.
2. Schindelin, H., Kisker, C., and Rajagopalan, K. V. (2001) *Adv. Protein Chem. 58*, 47−94.
3. Hille, R. (2002) in *Metal Ions in Biological Systems, Volume 39: Molybdenum and Tungsten: Their Roles in Biological Processes* (Sigel, A., and Sigel, H., Eds.) pp 187−226, Marcel Dekker, New York.
4. Johnson, J. L. (2003) *Prenatal Diagn.* 23, 6−8.
5. Dublin, A. B., Hald, J. K., and Wootton-Gorges, S. L. (2002) *Am. J. Neuroradiol. 23*, 484−485.
6. Johnson, J. L., Coyne, K. E., Garrett, R. M., Zabot, M.-T., Dorche, C., Kisker, C., and Rajagopalan, K. V. (2002) *Hum. Mutat. 20*, 74.
7. Johnson, J. L., Rajagopalan, K. V., Renier, W. O., Burgt, I., and Van der, Ruitenbeek, W. (2002) *Prenatal Diagn. 22*, 433−436.
8. Lee, H. F., Mak, B. S. C., Chi, C. S., Tsai, C. R., Chen, C. H., and Shu, S. G. (2002) *Neuropediatrics 33*, 174−179.
9. Lam, C. W., Li, C. K., Lai, C. K., Tong, S. F., Chan, K. Y., Ng, G. S. F., Yuen, Y. P., Cheng, A. W. F., and Chan, Y. W. (2002) *Mol. Genet. Metab. 75*, 91−95.
10. Garrett, R. M., Johnson, J. L., Graf, T. N., Feigenbaum, A., and Rajagopalan, K. V. (1998) *Proc. Natl. Acad. Sci. U.S.A. 95*, 6394−6398.
11. Kisker, C., Schindelin, H., Pacheco, A., Wehbi, W., Garrett, R. M., Rajagopalan, K. V., Enemark, J. H., and Rees, D. C. (1997) *Cell 91*, 973−983.
12. Hille, R. (1996) *Chem. Rev. 96*, 2757−2816.
13. Eilers, T., Schwarz, G., Brinkmann, H., Witt, C., Richter, T. Nieder, J., Koch, B., Hille, R., Hänsch, R., and Mendel, R. R. (2001) *J. Biol. Chem. 276*, 46989−46994.
14. Kappler, U., Bennett, B., Rethmeier, J., Schwarz, G., Deutzmann, R., McEwan, A. G., and Dahl, C. (2000) *J. Biol. Chem. 275*, 13202−13212.
15. Campbell, W. H. (1999) *Annu. Rev. Plant Physiol. Plant Mol. Biol. 50*, 277−303.
16. Rajagopalan, K. V. (1980) in *Molybdenum and Molybdenum-Containing Enzymes* (Coughlan, M. P., Ed.) pp 241−272, Pergmon, Oxford, UK.
17. Enemark, J. H., and Cosper, M. M. (2002) in *Metal Ions in Biological Systems, Volume 39: Molybdenum and Tungsten: Their Roles in Biological Processes* (Sigel, A., and Sigel, H., Eds.), pp 621−654, Marcel Dekker, NY.
18. Astashkin, A. V., Raitsimring, A. M., Feng, C., Johnson, J. L., Rajagopalan, K. V., and Enemark, J. H. (2002) *J. Am. Chem. Soc. 124*, 6109−6118.
19. Astashkin, A. V., Mader, M. L., Pacheco, A., Enemark, J. H., and Raitsimring, A. M. (2000) *J. Am. Chem. Soc. 122*, 5294−5302.
20. Raitsimring, A. M., Pacheco, A., and Enemark, J. H. (1998) *J. Am. Chem. Soc. 120*, 11263−11278.
21. Pacheco, A., Basu, P., Borbat, P., Raitsimring, A. M., and Enemark, J. H. (1996) *Inorg. Chem. 35*, 7001−7008.
22. Pacheco, A., Hazzard, J. T., Tollin, G., and Enemark, J. H. (1999) *J. Biol. Inorg. Chem. 4*, 390−401.
23. Sullivan, E. P., Jr., Hazzard, J. T., Tollin, G., and Enemark, J. H. (1993) *Biochemistry 32*, 12465−12470.
24. Sullivan, E. P., Jr., Hazzard, J. T., Tollin, G., and Enemark, J. H. (1992) *J. Am. Chem. Soc. 114*, 9662−9663.
25. Feng, C., Kedia, R. V., Hazzard, J. T., Hurley, J. K., Tollin, G., and Enemark, J. H. (2002) *Biochemistry 41*, 5816−5821.
26. Elliott, S. J., McElhaney, A. E., Feng, C., Enemark, J. H., and Armstrong, F. A. (2002) *J. Am. Chem. Soc. 124*, 11612−11613.
27. Leys, D., Basran, J., Talfournier, F., Sutcliffe, M. J., and Scrutton, N. S. (2003) *Nat. Struct. Biol. 10*, 219−225.
28. Hurley, J. K., Morales, R., Martinez-Julvez, M., Brodie, T. B., Medina, M., Gomez-Moreno, C., and Tollin, G. (2002) *Biochim. Biophys. Acta −Bioenerg. 1554*, 5−21.

29. Schlarb-Ridley, B. G., Bendall, D. S., and Howe, C. J. (2003) *Biochemistry 42*, 4057−4063.
30. Lushy, A., Verchovsky, L., and Nechushtai, R. (2002) *Biochemistry 41*, 11192−11199.
31. Tetreault, M., Cusanovich, M., Meyer, T., Axelrod, H., and Okamura, M. Y. (2002) *Biochemistry 41*, 5807−5815.
32. Kornilova, A. Y., Wishart, J. F., and Ogawa, M. Y. (2001) *Biochemistry 40*, 12186−12192.
33. Tetreault, M., Rongey, S. H., Feher, G., and Okamura, M. Y. (2001) *Biochemistry 40*, 8452−8462.
34. Hurley, J. K.; Faro, M.; Brodie, T. B.; Hazzard, J. T.; Medina, M.; Gomez-Moreno, C., and Tollin, G. (2000) *Biochemistry 39*, 13695−13702.
35. Temple, C. A., Tyler, N. G., and Rajagopalan, K. V. (2000) *Arch. Biochem. Biophys. 383*, 281−287.
36. Garrett, R. M., and Rajagopalan, K. V. (1996) *J. Biol. Chem. 271*, 7387−7391.
37. Leimkuhler, S., and Rajagoplan, K. V. (2001) *J. Biol. Chem. 276*, 1837−1844.
38. Garrett, R. M., and Rajagopalan, K. V. (1994) *J. Biol. Chem. 269*, 272−276.
39. Feng, C., Wilson, H. L., Hurley, J. K., Hazzard, J. T., Tollin, G., Rajagopalan, K. V., and Enemark, J. H. (2003) *J. Biol. Chem. 278*, 2913−2920.
40. Hurley, J. K., Weber-Main, A. M., Stankovich, M. T., Benning, M. M., Thoden, J. B., Vanhooke, J. L., Holden, H. M., Chae, Y. K., Xia, B., Cheng, H., Markley, J. L., Martínez-Júlvez, M., Gómez-Moreno, C., Schmeits, J. L., and Tollin, G. (1997) *Biochemistry 36*, 11100−11117.
41. Tollin, G. (2001) in *Electron Transfer in Chemistry* (Balzani, V., Ed.) Vol. 4, pp 202−231, Wiley-VCH, Weinheim.
42. Massey, V. (1959) *Biochim. Biophys. Acta 34*, 255−256.
43. Brody, M. S., and Hille, R. (1999) *Biochemistry 38*, 6668−6677.
44. Nicholls, A., Sharp, K., and Honig, B. (1991) *Proteins Struct. Funct. Genet. 11*, 281−296.
45. Hurley, J. K., Salamon, Z., Meyer, T. E., Fitch, J. C., Cusanovich, M. A., Markley, J. L., Cheng, H., Xia, B., Chae, Y. K., Medina, M., Gomez-Moreno, C., and Tollin, G. (1993) *Biochemistry 32*, 9346−9354.

BI0350194